Implementation, Verification and Validation of the Multi-Surface Failure Envelope for Ice in Explicit FEA (LS-DYNA) with Full Derivation of it's Invariant Form

Wang, Jungyong; Derradji-Aouat, Ahmed

http://dx.doi.org/10.4224/18227282

National Research Council Canada
Conseil national de recherches Canada
Institute for Ocean Technology
Institut des technologies océaniques

TR-2009-09

Technical Report

Implementation, Verification and Validation of the Multi-Surface Failure Envelope for Ice in Explicit FEA (LS-DYNA) with Full Derivation of it's Invariant Form.

Wang, J.; Derradji-Aouat, A.

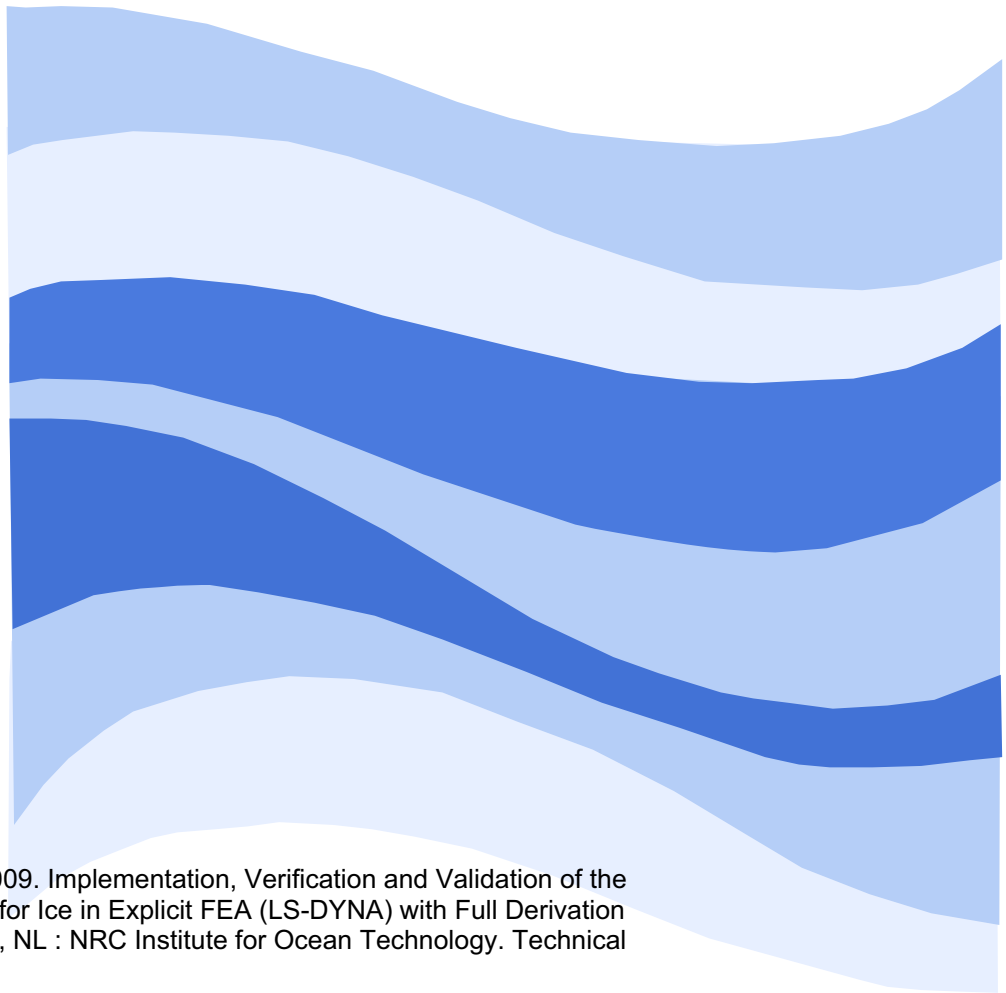

Wang, J.; Derradji-Aouat, A., 2009. Implementation, Verification and Validation of the Multi-Surface Failure Envelope for Ice in Explicit FEA (LS-DYNA) with Full Derivation of it's Invariant Form. St. John's, NL : NRC Institute for Ocean Technology. Technical Report, TR-2009-09.

Canada

DOCUMENTATION PAGE

REPORT NUMBER	NRC REPORT NUMBER	DATE
TR-2009-09		April 23, 2009
REPORT SECURITY CLASSIFICATION		**DISTRIBUTION**
Unclassified		Unlimited

TITLE

Implementation, Verification and Validation of the Multi-Surface Failure Envelope for Ice in Explicit FEA (LS-DYNA) with Full Derivation of its Invariant Form

AUTHOR(S)

Jungyong Wang and Ahmed Derradji-Aouat

CORPORATE AUTHOR(S)/PERFORMING AGENCY(S)

Institute for Ocean Technology, National Research Council, St. John's, NL

PUBLICATION

SPONSORING AGENCY(S)

IOT PROJECT NUMBER	NRC FILE NUMBER		
42-2335_26			
KEY WORDS	**PAGES**	**FIGS.**	**TABLES**
FEA, Failure envelope, Ice, LS-DYNA	iii, 15, App. 1	9	1

SUMMARY

The multi-surface failure criterion/model for ice is implemented into an explicit finite element program called LS-DYNA (www.lstc.com). The implementation of the model equations was achieved via the development of a user routine for LS-DYNA. Since ice behavior depends on temperature, strain/load rate and loading direction (loading direction for the case of anisotropic ice), the traditional isotropic and temperature and rate independent failure criterion such as von-Mises and Mohr-Coulomb are not applicable. The multi-surface failure criterion (Derradji-Aouat, 2003) accounts for those effects and is formulated with the parameters of the octahedral shear stress and hydrostatic pressure.

In this paper, a 3-step procedure will be presented and discussed to demonstrate successful multi-surface failure model implementation in explicit FEA. Step 1 is concerned with the theoretical implementation of the ice multi-surface failure model into the explicit commercial code LS-DYNA. Step 2 deals with verification and validation of the FE implementation, this step may be called V&V analysis and its rooted in uncertainty methodologies and statistical analyses. V&V will be based on comparisons between the numerical results and the results from the ice compression tests done by Rist and Murrell (1994) which was one of the data sources for the present failure criterion. Step 3 deals with showing how the implemented model in LS-DYNA predicts actual ice pressure and indentation tests on an ice block using the MTS machine in the cold room (Wells et al., 2008) and are simulated as an example. Discussion regarding the multi-surface model, its implementation, numerical results, and model predictions are presented.

ADDRESS National Research Council
Institute for Ocean Technology
Arctic Avenue, P. O. Box 12093
St. John's, NL A1B 3T5
Tel.: (709) 772-5185, Fax: (709) 772-2462

National Research Council Canada
Institute for Ocean Technology

Conseil national de recherches Canada
Institut des technologies océaniques

Implementation, Verification and Validation of the Multi-Surface Failure Envelope for Ice in Explicit FEA (LS-DYNA) with Full Derivation of its Invariant Form

TR-2009-09

Jungyong Wang and Ahmed Derradji-Aouat

April 2009

TABLE OF CONTENTS

Implementation, Verification and Validation of the Multi-Surface Failure Envelope for Ice in Explicit FEA (LS-DYNA) with Full Derivation of it's Invariant Form

Jungyong Wang and Ahmed Derradji-Aouat

Institute for Ocean Technology, National Research Council,

St. John's, Newfoundland, Canada

ABSTRACT

The multi-surface failure criterion/model for ice is implemented into an explicit finite element program called LS-DYNA (www.lstc.com). The implementation of the model equations was achieved via the development of a user routine for LS-DYNA. Since ice behavior depends on temperature, strain/load rate and loading direction (loading direction for the case of anisotropic ice), the traditional isotropic and temperature and rate independent failure criterion such as von-Mises and Mohr-Coulomb are not applicable. The multi-surface failure criterion (Derradji-Aouat, 2003) accounts for those effects and is formulated with the parameters of the octahedral shear stress and hydrostatic pressure.

In this paper, a 3-step procedure will be presented and discussed to demonstrate successful multi-surface failure model implementation in explicit FEA. Step 1 is concerned with the theoretical implementation of the ice multi-surface failure model into the explicit commercial code LS-DYNA. Step 2 deals with verification and validation of the FE implementation, this step may be called V&V analysis and its rooted in uncertainty methodologies and statistical analyses. V&V will be based on comparisons between the numerical results and the results from the ice compression tests done by Rist and Murrell (1994) which was one of the data sources for the present failure criterion. Step 3 deals with showing how the implemented model in LS-DYNA predicts actual ice pressure and indentation tests on an ice block using the MTS machine in the cold room (Wells et al., 2008) and are simulated as an example. Discussion regarding the multi-surface model, its implementation, numerical results, and model predictions are presented.

INTRODUCTION

In these days, ships navigating in ice-covered water are more and more important because shipping activities in Arctic/sub-Arctic regions have been rapidly increased for the transportation of natural resources, and the Northern Sea Route may open soon due to the global warming. Unlike an offshore structure, a ship moves at a certain speed and the failure of ice by the ship is much different from that by the offshore structure. The reason is that the ice failure is dependent on loading rate. For the sake of explanation, the engineering strain rate $\dot{\varepsilon} = V / 4D$ is used to determine the strain rate for a typical ship speed (Cammaert and Muggeridge, 1988, p.228). For example, when a ship has the forward speed of 5 knots and the maximum beam of 20 m, the

engineering strain rate is equal to 0.03/s. Generally speaking, if $\dot{\varepsilon} \rangle 1\times10^{-3}/s$ then the dominant ice failure occurs in the brittle regime. Therefore, the reasonable prediction of ice in the brittle failure regime would be needed and its constitutive modelling for the numerical simulation is required.

A Finite Element (FE) numerical modelling with an appropriate constitutive equation (stress-strain relation) for ice enables us to predict the overall performance of a ship in any ice condition. In addition, FE modelling makes it possible to assess the risk in a wide range of operational scenarios including an extreme condition such as ship-ice, ship-ship and ship-structure collisions, which may be beyond the limitation of model tests. Clearly, it will significantly help to update/modify a regulatory body in ice covered water with regard to safety, design and operational guidance. Therefore, the development of an accurate numerical modelling technology plays a major role in the cost-effective performance prediction and risk assessment of ships in ice.

Mathematical modelling of ice deformation behaviour in continuum mechanics using elasto-plastic, viscoplastic or viscoelastic flow has been formulated as a constitutive model of ice (Sinha, 1978; Pulkkinen, 1988; Fish, 1992; Derradji-Aouat, 1992, 2000). These models, however, were based on the creep tests in the low strain rate condition ($\dot{\varepsilon} \langle 1\times10^{-3}/s$), and represented a ductile failure mode associated with dense microcracking and recrystallization rather than a brittle failure mode with macrocracking and fracture. For the latter matters, fracture mechanics and damage mechanics were generally considered (Pulkkinen, 1988; Choi, 1989; Derradji-Aouat, 2005).

In this paper, we considered the continuum mechanics and brittle failure regime only at the high strain rate ($\dot{\varepsilon} \rangle 5\times10^{-3}/s$). This paper aimed to implement an existing constitutive model of ice into the explicit finite element code (LS-DYNA) and to validate the implementation. The constitutive model of ice presented in this paper was developed for the brittle regime at the high strain rate by Derradji-Aouat (2003). For the validation purpose, a cylinder shaped ice compression test was simulated and compared with the results from Rist and Murrell (1994). For the application, the ice block indentation test was simulated and the numerical results were compared with those from cold room tests (Wells et al., 2008) and followed by discussion.

MULTI-SURFACE FAILURE CRITERIA

The concept of the multi-surface failure criterion is briefly introduced and the equations implemented into LS-DYNA are shown in this section. The main idea of a multi-surface failure criterion is to represent the failure envelope with the parameters of octahedral shear stress and hydrostatic pressure (τ_{oct} - p plot, see Fig. 1). Derradji-Aouat (2003) compiled the triaxial test data from Jones (1982) and Rist and Murrell (1994), and he formulated the equation of the 2-D elliptic failure envelope as shown in Eq. 1.

$$\left(\frac{\tau_{oct}-\eta}{\tau_{oct\_\max}}\right)+\left(\frac{p-\lambda}{P_{c\_\max}}\right)=1 \qquad (1)$$

where τ_{oct} and p are the octahedral shear stress in the minor axis and hydrostatic pressure (same as the confining pressure, P_c) in the major axis, and η and λ are the coordinates for the center of the ellipse.

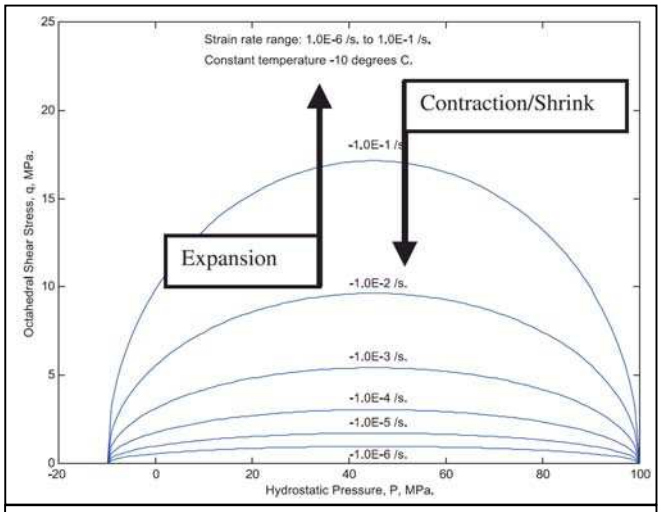

Fig. 1: τ_{oct} - p plot from Derradji-Aouat (2003), it shows the elliptic failure envelope with various strain rates

In a typical triaxial test, lateral pressure at two axes (x-2 and x-3) was the same as the confining pressure P_c, i.e. $\sigma_2=\sigma_3=P_c$ (see Fig. 2). Therefore, Eq. 1 can be extended to the 3-D, which is a circular ellipsoid and the general equation is shown in Eq. 2.

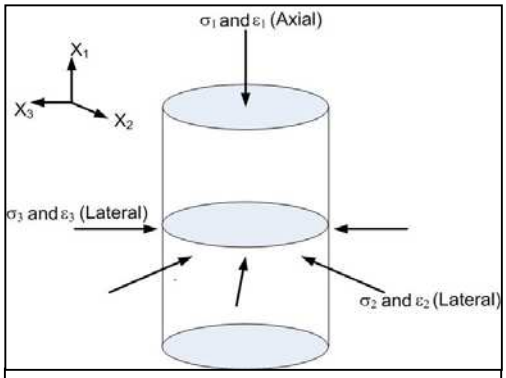

Fig. 2: A schematic of triaxial loading direction

$$\left(\frac{(p^*-\alpha)}{a}\right)^2+\left(\frac{(s-\beta)}{b}\right)^2+\left(\frac{(s'-\gamma)}{c}\right)^2=1 \qquad (2)$$

where $a=P_{c\_\max}, b=c=\tau_{oct\_\max}$, $\alpha=\lambda=45MPa$ for freshwater/iceberg ice.

In order to determine $\tau_{oct\_\max}$, the formula addressed in Derradji-Aouat (2000) was used (see Eq. 3). Since this paper is focused on the implementation of the existing constitutive model, for the detailed explanation of the constitutive equation, see the Derradji-Aouat (2000) and Wang and Derradji-Aouat (2009).

$$\tau_{oct\_\max}=\left(\frac{\dot{\varepsilon}}{\xi}\right)^{1/n} \qquad (3)$$

where

$n=4$, $\xi=5\times10^{-6}\exp\left[-10.5\times10^{3}\left(\frac{1}{T}-\frac{1}{273}\right)\right]$

It can be re-written as an invariant form as shown in Eq. 4.

$$\frac{8}{3b^2}J_{2D}+\frac{2}{3b^2}I_2+\frac{1}{9}\left(\frac{1}{a^2}-\frac{2}{b^2}\right)I_1^{\,2}+\frac{2\alpha}{3a^2}I_1+\frac{\alpha^2}{a^2}=1 \qquad (4)$$

where, I_1, I_2, and J_{2D} are the first, second stress invariants, and the second deviatoric stress invariants. Other parameters are the same as those in Eq. 2. Full derivation is addressed in

Appendix 1. In the invariant form, Eq. 4 is always valid regardless a coordinate system. Eq. 4 indicates that if the value from the left hand side is equal or bigger than 1, then the element reaches the failure.

IMPLEMENTATION INTO LS-DYNA

In the brittle regime, ice acts as a linear elastic material before a failure occurs. Most likely the failure is caused by a fracture or macrocracking, so that the load vs. time or stress vs. strain curves show a sharp drop of the load or stress. There are two ways to implement a user defined material in LS-DYNA (LS-DYNA971 Manual). First, if only a failure criterion needs to be implemented and the material behaves elastic and/or plastic before the failure, then using an elasto-plastic materal (MAT_024, piecewise linear plasticity material) is the most convenient. Second, if a new stress-strain relationship needs to be implemented, then using one of the 10 empty user defined material slots (MAT_041- MAT_050) can be used. The present study used Mat_024 and the multi-surface failure criterion as described in Eq. 4 was implemented. In the Mat_024, the yield stress had to be set high enough (0.1Gpa, which is bigger than failure shear stress) to avoid any plastic behavior. At each time step, all stresses on each element were evaluated. If the calculated stress on the element reaches the failure envelope, then the element is set to be failed and eroded (removed). Element eroding may not be appropriate because the elements are not physically removed in the real world but possibly changed their status due to pressure melting, pulverization, plastic hardening/softening, and fracture. Since the main objective is to implement the failure criterion in LS-DYNA, eroding contact is one of the convenient options as a preliminary calculation stage. For the contact option, "Contact_Eroding_Nodes_To_ Surface" which can re-establish the surface shape once the erosion of the element was occurred and the contact surface was changed. Table 1 shows the input parameters for the present numerical simulations.

Table 1: Input parameters for the numerical simulation

	$P_{c\_\max} = a$	$\tau_{oct\_\max} = b = c$	$\alpha = \lambda$	E
Rist and Murrell (1994), $T = -40^{o}C,\ \dot{\varepsilon} = 0.01/s$	55 MPa	34.8 MPa	45 MPa	6.4 GPa
Wells et al. (2008), $T = -10^{o}C,\ \dot{\varepsilon} = 0.1/s$	55 MPa	17.1 MPa	45MPa	6.0 GPa

VERIFICATION AND VALIDATION

In order to validate the present simulation model with implemented failure criterion, one of the triaxial tests from Rist and Murrell (1994) is simulated. Since their data was one of the source data for the present failure envelope, it would be a good indicator for an adequate validation. Fig. 3 shows the numerical model for the simulation. The top blue cap is a rigid body to compress the cylinder shaped ice specimen (red colour) below. About total 11,000 elements were used and the

bottom of the ice specimen was fixed. The cap part had a downward velocity of 0.001 m/s, which is corresponding to the strain rate of 0.01 /s and the hydrostatic pressure (confining pressure, P_c) of 10 MPa was applied in the outer surface of the ice specimen.

Fig. 4 shows the maximum shear stress on the ice specimen. The simulation is still in progress and fracture/macrocracking behaviour is not shown from the present simulation at this moment. The stress comparison is made as shown in Fig. 5. The left figure in Fig. 5 shows the experimental result from Rist and Murrell (1994) and the right figure presents the numerical result. Because the confining pressure of 10 MPa was applied in all directions, the differential stress in the axial direction ($\sigma_1 - \sigma_3$) is compared to that from experiments. Since the failure criterion has a circular ellipsoid and the maximum failure stress is assumed to occur at P_c = 55 MPa, the maximum stress with the confining pressure of 10 MPa should be higher than those at without the confining pressure. The result shows that the maximum differential stress from numerical prediction is about 10 MPa less than that from the experiments.

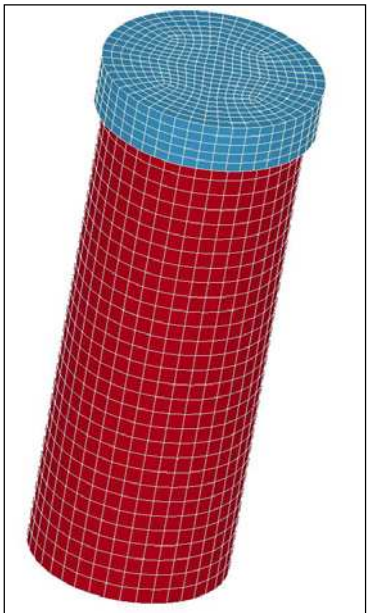

Fig. 3: Numerical model of triaxial tests

The data from Rist and Murrell (1994) included a wide range of the strain rate ($10^{-5} \sim 10^{-2}$/s) and most ice samples failed in ductile mode: some of them had a ductile failure even in the highest strain rate ($\dot{\varepsilon} = 10^{-2}$) at the temperature of $-20^{o}C$. While the experimental result was used for the brittle regime only, the present constitutive model was established from the whole range of the strain rate ($\dot{\varepsilon} = 10^{-5} \sim 10^{-2}$/s) including data from Jones (1982). It may cause the discrepancy of 10 MPa between experimental and numerical results. For a better prediction at the high strain rate condition, such as the ship operating condition, ice triaxial test data for the wide range of high strain rate ($\dot{\varepsilon} = 10^{-2} \sim 10^{1}$/s) must be used to improve the present constitutive modelling. Fracture behaviour seems to play an important role in the whole simulation process, so that this feature needs to be included in the constitutive model.

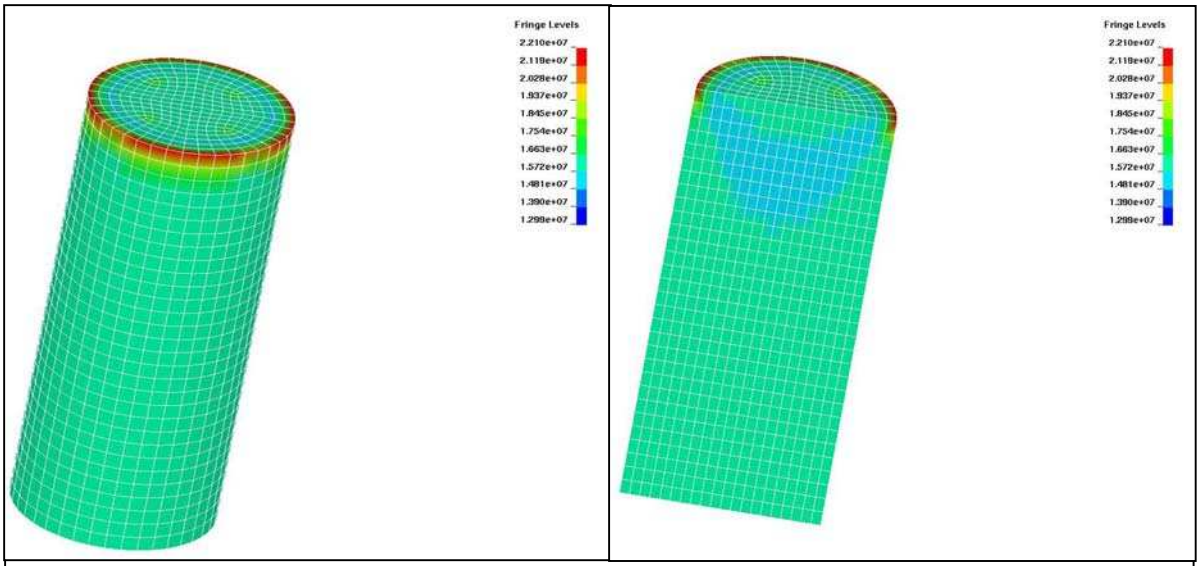

Fig. 4: (left) Maximum shear stress just before failure; (right) Maximum shear stress distribution in the centre plane

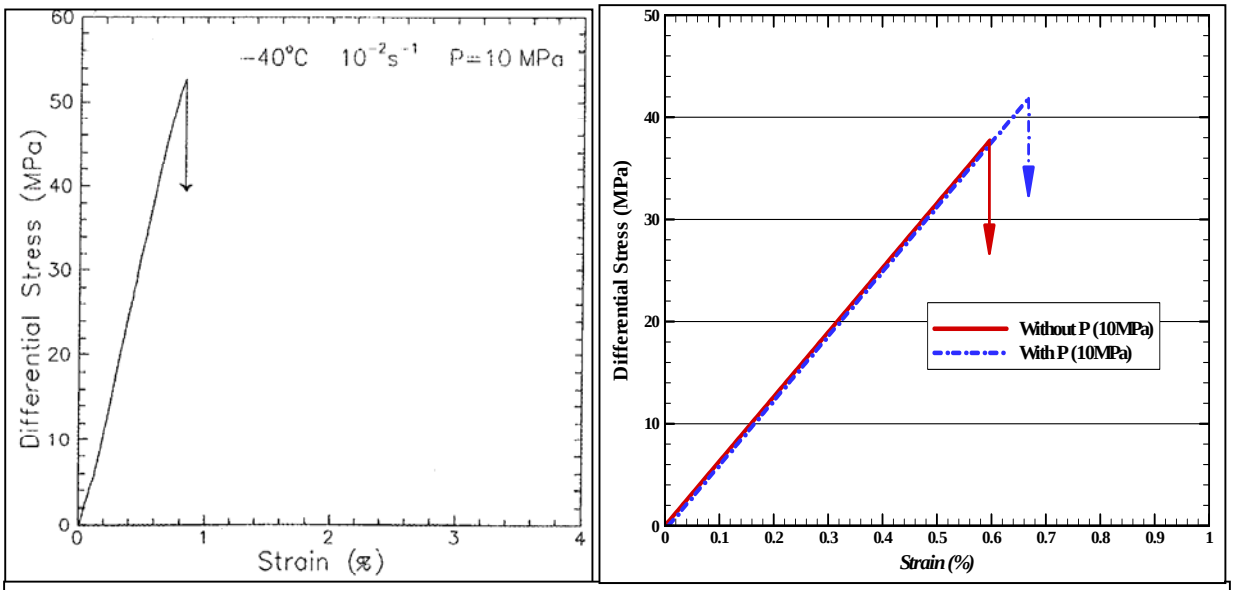

Fig. 5: Comparison of results from Rist and Murrell (1994) and those from numerical simulation with/without confining pressure (P_c)

APPLICATION

The implemented multi-failure surface criterion is applied to predict the pressure from ice indentation tests done by Wells et al. (2008) at the IOT's cold room. The purpose of the tests was to investigate the fracture behavior of polycrystalline ice with/without an embedded mono crystal. The dimension of the ice specimens was $20\times 20\times 10$ cm and polycrystalline ice with a grain size of about 4 mm. As an indentor, a 20 mm long rigid cylinder with a curved bottom was used and it indented the ice block in two different locations (centre, and between centre and edge). The range of the indentor speed and strain rate was from 0.2 mm/s to 10mm/s and 1.8E-3/s to 1.0E-2/s, respectively. The detailed explanation of ice specimen preparation and the test condition was given in Wells et al. (2008).

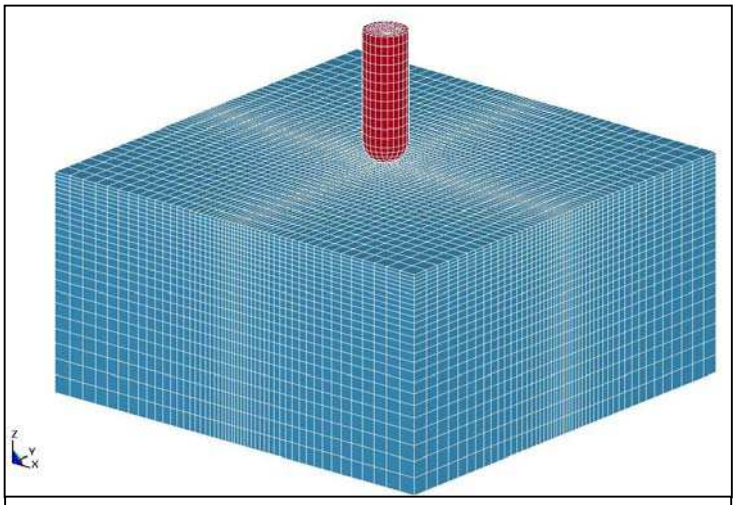

Fig. 6: Numerical simulation of ice indentation tests: top- rigid cylindrical indentor; bottom- ice block

For the numerical simulation, the indentor is located at the centre of the ice block, and the indentor speed of 10mm/s (corresponding strain rate of 0.1/s) is used. In order to reduce a calculation time, the size of the numerical model is three times bigger than that of the physical

model. For the small contact area range from 2.5cm^2 to 2500 cm^2, the peak pressure of the prototype and that of three orders of magnitude in scale would be the same (Gagnon, 1999). For a FE calculation, mesh size plays a major role in the calculation time; i.e. if the mesh size is too small, it takes much longer time because of a small time step. The time step size roughly corresponds to the transient time of an acoustic wave through an element using the shortest characteristic distance (from LS-DYNA 971 User Manual). Therefore, for the numerical model, the ice block dimension of $60 \times 60 \times 30$ cm is used as shown in Fig. 6. Total about 70,000 elements are used and the calculation time with two CPUs (each CPU has 2 GHz processor with 6 G Ram) is about 55 hours for one (1) second simulation time. Most stress/pressure is expected to concentrate in the centre where the denser mesh was used. Maximum pressure from the experiments is compared with that from the present simulation.

Fig. 7 shows the maximum effective stress contours at 0.235 and 0.72 seconds. The reason to select these times is to show one of the peak stresses because at the next time step, the elements reached the failure criterion and eroded/removed. Fig. 8 shows the maximum pressure calculated from the top surface to sixth layer below because the element eroding occurred up to sixth layer.

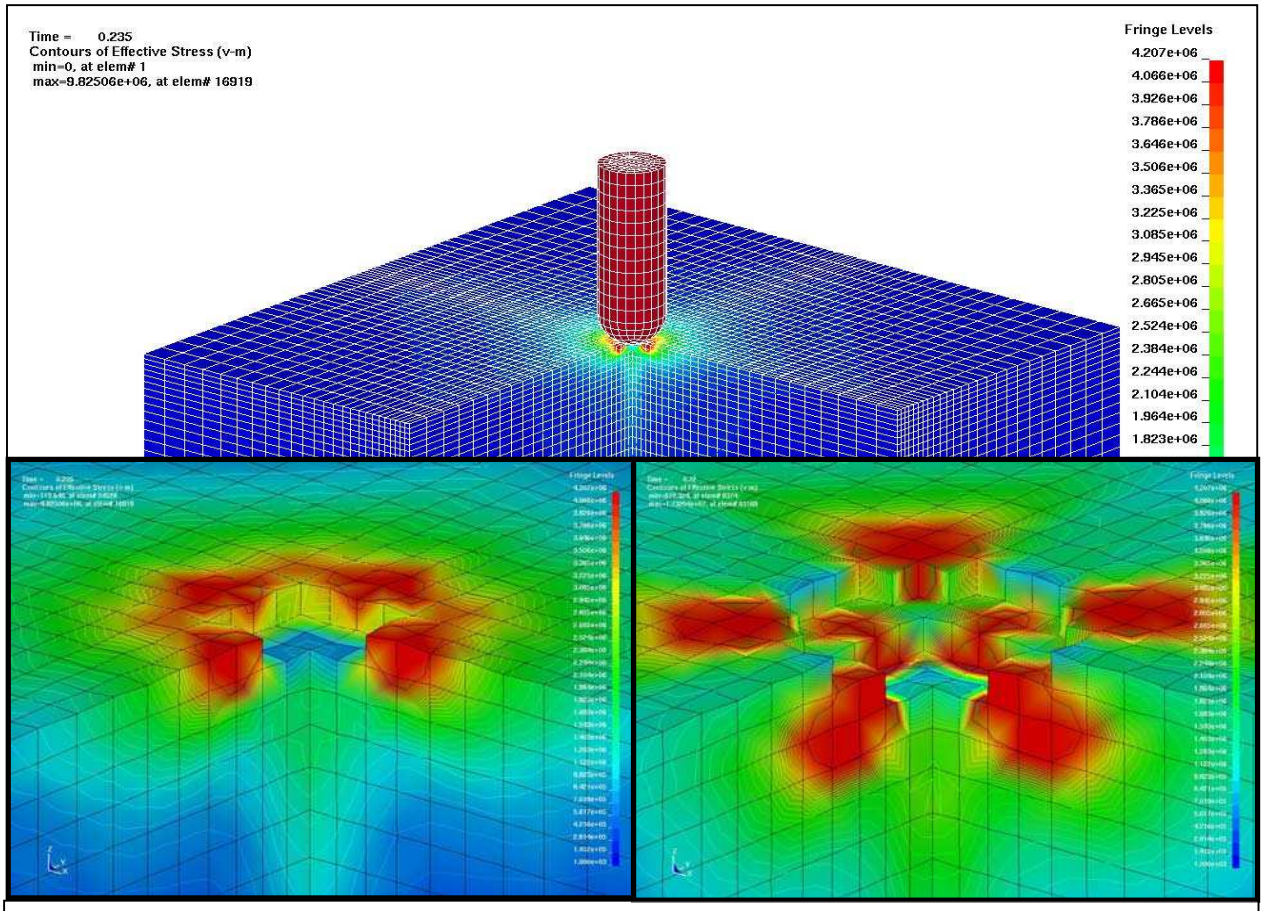

Fig. 7: Maximum effective stress contours; (top center) both indentor and ice block are shown at 0.235 sec, one fourth ice block was removed to see inside; (bottom left) the zoom-in contact area at 0.235 sec; (bottom right) the zoom-in contact area at 0.72 sec, hollow part in the centre indicates the elements reached the failure criterion and removed/eroded; the indentor is not shown in the bottom figures

In Fig. 8, almost zero pressure was found right after pressure drops. This is because the elements were eroded before the indentor reached the next elements. Element eroding may be not the best option to simulate this indentation test because the elements are not physically removed in real world but possibly changed their status due to pressure melting, pulverization, plastic hardening/softening, and fracture. Eroding contact option needs to be improved in order to take into account these effects.

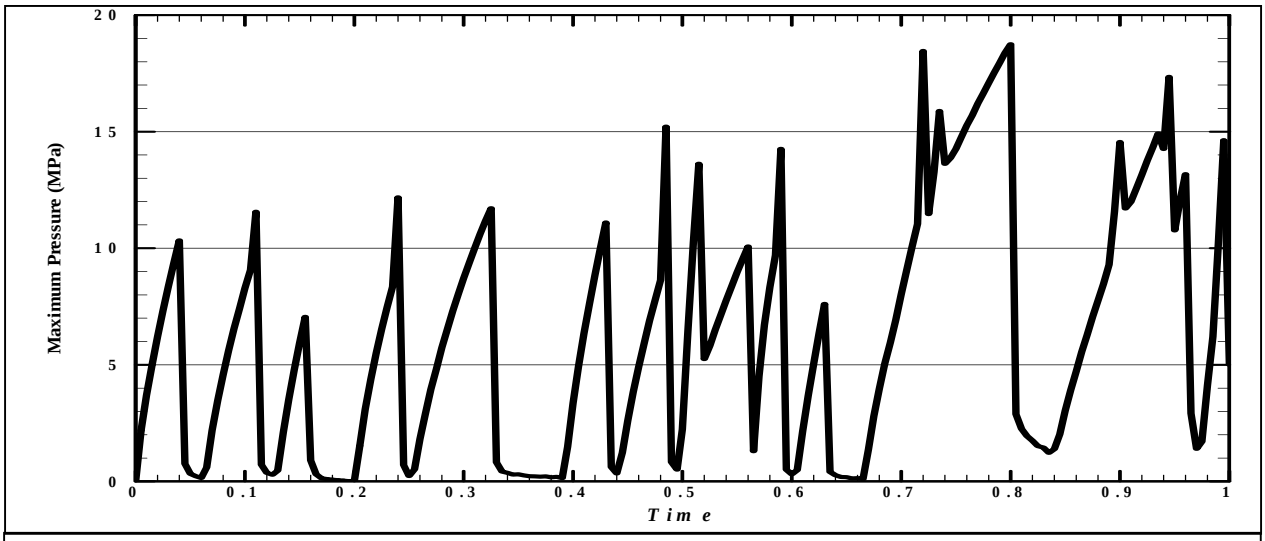

Fig. 8: Maximum pressure calculated from the top surface to sixth layer below

Fig. 9 shows the experimental results from Well et al. (2008). In the experiments, the maximum pressure varied from 30 to 60 MPa, but the numerical result showed about 10 - 18 MPa. In the nominal stress graph (bottom in Fig. 9), sudden drops due to macrocracking and fracture were observed.

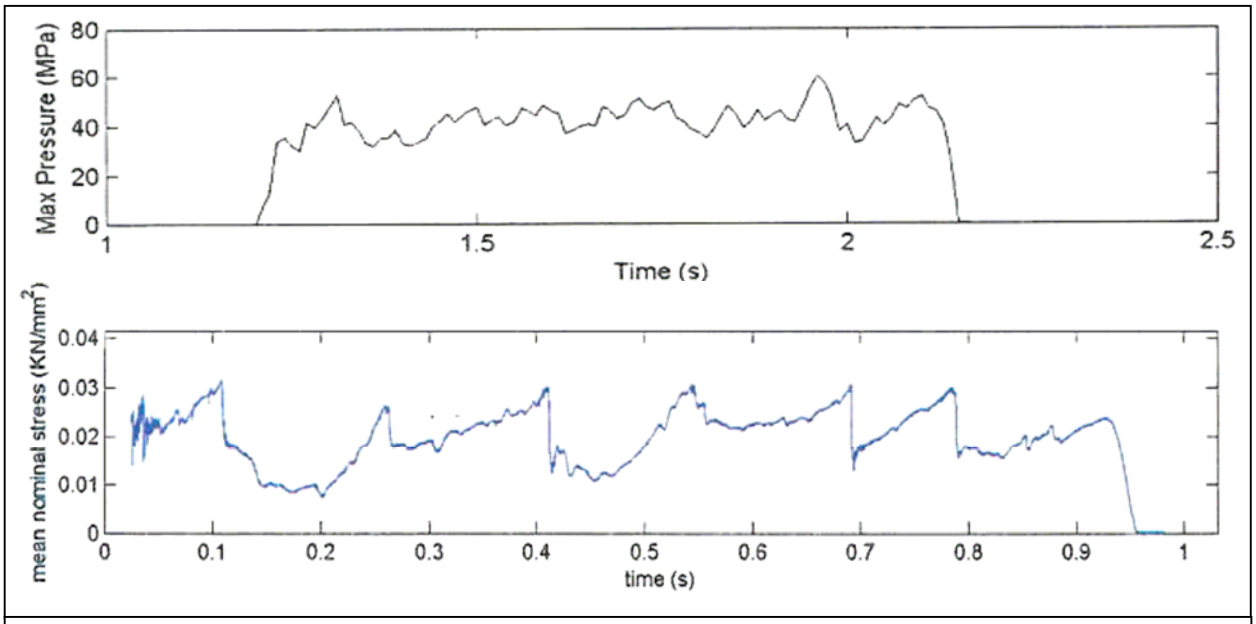

Fig. 9: Results from experiments (Wells et al., 2008)

CONCLUSION

In this paper, the constitutive model for ice was successfully implemented into the Explicit Finite Element code (LS-DYNA) using the elasto-plastic material (MAT_024) with a user-defined failure criterion (multi-surface failure criterion). In order to avoid any plastic behaviour, we set the high yield stress value (0.1Gpa, which is bigger than failure shear stress) as an input of MAT_024. The τ_{oct} - p multi surface failure theory implemented into LS-DYNA worked well even though there is a discrepancy in the magnitude between the numerical simulation and experimental test. We expect that it is because the constitutive model for ice was developed from the wide range of strain rate ($\dot{\varepsilon} = 10^{-5} \sim 10^{-2}$/s) that includes a ductile failure, while only brittle regime data from the experiments were used for comparison. In order to improve the constitutive model for ice in the brittle regime the data from triaxial compression tests at the high strain rate ($\dot{\varepsilon} = 10^{-2} \sim 10^{1}$/s) with uncertainty analysis are necessary. Since the fracture behaviour was not simulated at this moment, fracture model may need to be combined with the present model.

REFERENCES

Cammaert, A. B. and Muggeridge, D. B., 1988. Ice Interaction with Offshore Structures, New York: Van Nostrand Reinhold, 432p.

Choi, K., 1989. A damage mechanics approach to the three dimensional constitutive modelling of ice deformation. Ph.D. Thesis, Massachusetts Institute of Technology, Dept. of Ocean Eng. 175p.

Derradji-Aouat, A., 2003. Multi-surface failure criterion for saline ice in the brittle regime. Cold Regions Science and Technology, 36 (1-3): 47-70.

Derradji-Aouat , A., 1992. Mathematical modelling of monotonic and cyclic behaviour of polycrystalline fresh water ice. Ph.D. Thesis, University of Ottawa, Dept. of Civil Eng. 197p.

Derradji-Aouat, A., 2000. A unified failure envelope for isotropic freshwater ice and iceberg ice. ASME/OMAE-2000, International Conference on Offshore Mechanics and Arctic Engineering, Polar and Arctic section, New Orleans, US, PDF file # OMAE-2000- P/A # 1002.

Derradji-Aouat, A., 2005. Explicit FEA and constitutive modelling of damage and fracture on polycrystalline ice - simulations of ice loads on offshore structures. 18th International Conference on Port and Ocean Engineering Under Arctic Conditions, 26-30 June 2005, Potsdam, New York. p. 225-238

Fish, A. M., 1992. Three-dimensional viscoplastic flow model of polycrystalline ice. Int. Conference on Ice Technology, Massachusetts Institute of Technology. pp.193-207.

Gagnon, R. E., 1999. Consistent observations of ice crushing in laboratory tests and field experiments covering three orders of magnitude in scale. 15th International Conference on Port and Ocean Engineering Under Arctic Conditions, 23-27 August 1999, Espoo, Finland. p. 859-869.

Jones, S. J., 1982. The confined compressive strength of polycrystalline ice. Journal of Glaciology. Vol. 28, No. 98, pp.171–177.

LS-DYNA 971 Keyword User's Manual, LSTC, (www.lstc.com)

Pulkkinen, E., 1988. Numerical modelling of ice behaviour. Ph.D. Thesis, University of Oulu, Dept. of Mech. Eng. 112p.

Rist, M. A. and Murrell, S. A. F., 1994. Ice triaxial deformation and fracture. Journal of Glaciology, Vol. 40, No. 135, pp. 305-318.

Sinha, N. K., 1978. Rheology of columnar grained ice. Experimental mechanics, Vol. 18, No. 12, pp. 464-470.

Wells, J., Derredji-Aouat, et al., 2008. Laboratory investigation of the fracture behaviour of polycrystalline ice: Phase II. Institute for Ocean Technology, St. John's, Canada, Report # TR-2008-08, 179p.

Appendix 1

Derivation of Invariant Form

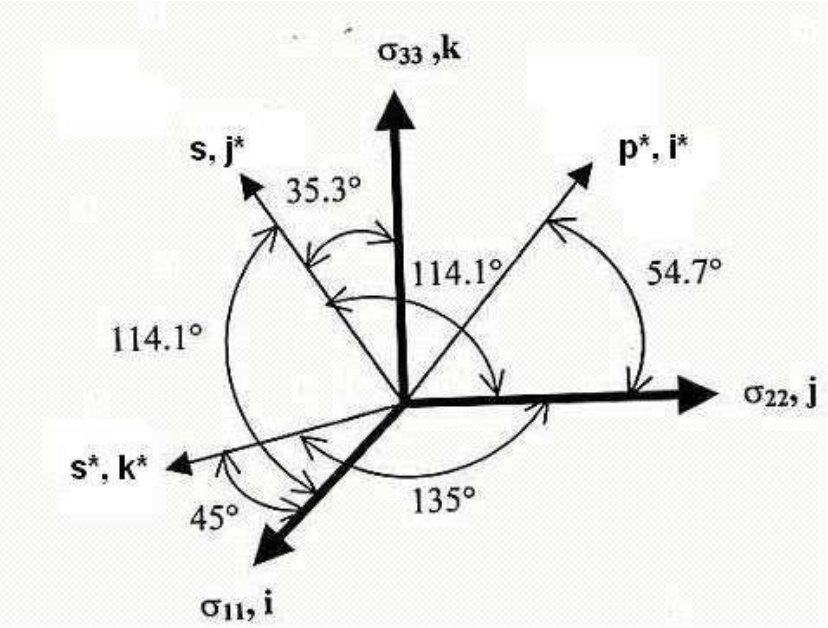

Figure 1-1: Coordinate transformation

In Fig.1-1, a principal stress plane ($\sigma_1, \sigma_2, \sigma_3$) can be transformed into a failure plane (p^*, s, s'). p^* is the hydrostatic pressure axis. Shear stresses (s and s') are laid on the deviatoric plane (π-plane) and which are perpendicular to p^* and each other to form a Cartesian coordinate.

Transformation matrix is shown in below.

$$\begin{bmatrix} p^* \\ s \\ s' \end{bmatrix} = [T] \begin{bmatrix} \sigma_1 \\ \sigma_2 \\ \sigma_3 \end{bmatrix} \text{ and } \quad [T] = \begin{bmatrix} \frac{1}{\sqrt{3}} & \frac{1}{\sqrt{3}} & \frac{1}{\sqrt{3}} \\ \frac{-1}{\sqrt{6}} & \frac{-1}{\sqrt{6}} & \frac{\sqrt{2}}{\sqrt{3}} \\ \frac{1}{\sqrt{2}} & \frac{-1}{\sqrt{2}} & 0 \end{bmatrix} \tag{1}$$

The failure surface is shown in a circular ellipsoid and the general formulation of an ellipsoid is shown in Eq. 2.

$$\left(\frac{(p^* - \alpha)}{a}\right)^2 + \left(\frac{(s - \beta)}{b}\right)^2 + \left(\frac{(s' - \gamma)}{c}\right)^2 = 1 \tag{2}$$

where *a* and *b* are the equatorial radii (along the p^* and *s* axes) and *c* is the polar radius (along the s' axis). From the failure surface, the hydrostatic pressure p^* is considered as positive when the model was compressed. Therefore the hydrostatic pressure needs to be changed as $p^* = -p$. The coordinate of (α, β, γ) is the centre of the ellipsoid.

In the proposed failure surface, β and γ are equal to zero and $b = c$ due to the circular ellipsoid. Therefore we get the eq.3.

$$\frac{s^2 + s'^2}{b^2} = \left(1 - \frac{(-p-\alpha)^2}{a^2}\right) \tag{3}$$

Now Eq.1 is equated in terms of stress components. $s^2 + s'^2$ in the LHS of eq. 3 is to be:

$$\left(\frac{-1}{\sqrt{6}}\sigma_{11} + \frac{-1}{\sqrt{6}}\sigma_{22} + \frac{\sqrt{2}}{\sqrt{3}}\sigma_{33}\right)^2 + \left(\frac{1}{\sqrt{2}}\sigma_{11} + \frac{-1}{\sqrt{2}}\sigma_{22}\right)^2$$

$$= \left(\frac{1}{6}\sigma_{11}{}^2 + \frac{1}{6}\sigma_{22}{}^2 + \frac{2}{3}\sigma_{33}{}^2 + \frac{1}{3}\sigma_{11}\sigma_{22} + \frac{-2}{3}\sigma_{22}\sigma_{33} + \frac{-2}{3}\sigma_{11}\sigma_{33}\right) + \left(\frac{1}{2}\sigma_{11}{}^2 - \sigma_{11}\sigma_{22} + \frac{1}{2}\sigma_{22}{}^2\right)$$

$$= \frac{2}{3}\sigma_{11}{}^2 + \frac{2}{3}\sigma_{22}{}^2 + \frac{2}{3}\sigma_{33}{}^2 + \frac{-2}{3}\sigma_{11}\sigma_{22} + \frac{-2}{3}\sigma_{22}\sigma_{33} + \frac{-2}{3}\sigma_{11}\sigma_{33}$$

Therefore Eq.3 is to be:

$$\frac{2}{3b^2}\left(\sigma_{11}{}^2 + \sigma_{22}{}^2 + \sigma_{33}{}^2 - (\sigma_{11}\sigma_{22} + \sigma_{22}\sigma_{33} + \sigma_{11}\sigma_{33})\right) = \left(1 - \frac{(-p-\alpha)^2}{a^2}\right) \tag{4}$$

It is noted that there are no shear stress terms after the transformation into the failure surface. It means this coordinate is the same as the principal stress axes. Since the invariants of the stress tensors are the same regardless the coordinate system, we introduce the invariant terms now.

The parenthesis of LHS in the Eq. 4 can be rearranged with Eqs 4.1,4.2, and 4.3

$$\frac{1}{2}(\sigma_{11}{}^2 + \sigma_{22}{}^2 + \sigma_{33}{}^2) - \frac{1}{6}(\sigma_{11} + \sigma_{22} + \sigma_{33})^2 + \sigma_{12}{}^2 + \sigma_{23}{}^2 + \sigma_{31}{}^2 \quad ---(4.1)$$

$$+\frac{1}{2}(\sigma_{11}{}^2 + \sigma_{22}{}^2 + \sigma_{33}{}^2) + \frac{1}{6}(\sigma_{11} + \sigma_{22} + \sigma_{33})^2 - (\sigma_{12}{}^2 + \sigma_{23}{}^2 + \sigma_{31}{}^2) ---(4.2)$$

$$-(\sigma_{11}\sigma_{22} + \sigma_{22}\sigma_{33} + \sigma_{33}\sigma_{11}) ----------(4.3)$$

In Eq. 4.1

$$\frac{1}{2}(\sigma_{11}{}^2+\sigma_{22}{}^2+\sigma_{33}{}^2)-\frac{1}{6}(\sigma_{11}+\sigma_{22}+\sigma_{33})^2+\sigma_{12}{}^2+\sigma_{23}{}^2+\sigma_{31}{}^2$$
$$=\frac{1}{6}\left(3\sigma_{11}{}^2+3\sigma_{22}{}^2+3\sigma_{33}{}^2-\sigma_{11}{}^2-\sigma_{22}{}^2-\sigma_{33}{}^2-2\sigma_{11}\sigma_{22}-2\sigma_{22}\sigma_{33}-2\sigma_{33}\sigma_{11}\right)+\sigma_{12}{}^2+\sigma_{23}{}^2+\sigma_{31}{}^2$$
$$=\frac{1}{6}\left(2\sigma_{11}{}^2+2\sigma_{22}{}^2+2\sigma_{33}{}^2-2\sigma_{11}\sigma_{22}-2\sigma_{22}\sigma_{33}-2\sigma_{33}\sigma_{11}\right)+\sigma_{12}{}^2+\sigma_{23}{}^2+\sigma_{31}{}^2$$
$$=\frac{1}{6}\left((\sigma_{11}-\sigma_{22})^2+(\sigma_{22}-\sigma_{33})^2+(\sigma_{33}-\sigma_{11})^2\right)+\sigma_{12}{}^2+\sigma_{23}{}^2+\sigma_{31}{}^2$$
$$=J_{2D}$$

In Eqs.4.2 and 4.3

$$\frac{1}{2}(\sigma_{11}{}^2+\sigma_{22}{}^2+\sigma_{33}{}^2)+\frac{1}{6}(\sigma_{11}+\sigma_{22}+\sigma_{33})^2-(\sigma_{12}{}^2+\sigma_{23}{}^2+\sigma_{31}{}^2)-(\sigma_{11}\sigma_{22}+\sigma_{22}\sigma_{33}+\sigma_{33}\sigma_{11})$$
$$=\frac{1}{2}(\sigma_{11}{}^2+\sigma_{22}{}^2+\sigma_{33}{}^2)+(\sigma_{11}+\sigma_{22}+\sigma_{33})^2-(\sigma_{12}{}^2+\sigma_{23}{}^2+\sigma_{31}{}^2)-\frac{5}{6}(\sigma_{11}+\sigma_{22}+\sigma_{33})^2$$
$$-(\sigma_{11}\sigma_{22}+\sigma_{22}\sigma_{33}+\sigma_{33}\sigma_{11}) \quad ----(4.4)$$

Since $I_2=\sigma_{11}\sigma_{22}+\sigma_{22}\sigma_{33}+\sigma_{33}\sigma_{11}-(\sigma_{12}{}^2+\sigma_{23}{}^2+\sigma_{31}{}^2)$,

Eq.4.4 is

$$\frac{1}{2}(\sigma_{11}{}^2+\sigma_{22}{}^2+\sigma_{33}{}^2)+(\sigma_{11}{}^2+\sigma_{22}{}^2+\sigma_{33}{}^2+2\sigma_{11}\sigma_{22}+2\sigma_{22}\sigma_{33}+2\sigma_{11}\sigma_{33})$$
$$-(\sigma_{12}{}^2+\sigma_{23}{}^2+\sigma_{31}{}^2)-\frac{5}{6}(\sigma_{11}+\sigma_{22}+\sigma_{33})^2-(\sigma_{11}\sigma_{22}+\sigma_{22}\sigma_{33}+\sigma_{33}\sigma_{11})$$
$$=\frac{3}{2}(\sigma_{11}{}^2+\sigma_{22}{}^2+\sigma_{33}{}^2)+I_2-\frac{5}{6}I_1{}^2$$

Since $p=\frac{1}{3}(\sigma_{11}+\sigma_{22}+\sigma_{33})=\frac{I_1}{3}$, the RHS of Eq. 4 is to be

$$\left(1-\frac{(-p-\alpha)^2}{a^2}\right)=\left(1-\frac{\frac{I_1{}^2}{9}+\frac{2\alpha I_1}{3}+\alpha^2}{a^2}\right)=1-\frac{I_1{}^2}{9a^2}-\frac{2\alpha I_1}{3a^2}-\frac{\alpha^2}{a^2} \qquad (5)$$

Therefore, Eq.4 is

$$\frac{2}{3b^2}\left(J_{2D}+\frac{3}{2}(\sigma_{11}{}^2+\sigma_{22}{}^2+\sigma_{33}{}^2)+I_2-\frac{5}{6}I_1{}^2\right)=1-\frac{I_1{}^2}{9a^2}-\frac{2\alpha I_1}{3a^2}-\frac{\alpha^2}{a^2} \qquad (6)$$

As mentioned earlier, because this coordinate is the same as the principal stress axes, we refer the stresses as the principal stresses ($\sigma_1, \sigma_2, \sigma_3$). If we rearrange the parenthesis of the LHS in the Eq. 6,

$$J_{2D} + \frac{3}{2}(\sigma_1^{\,2} + \sigma_2^{\,2} + \sigma_3^{\,2}) + I_2 - \frac{5}{6} I_1^{\,2} \tag{7}$$

$$\begin{aligned}\sigma_1^{\,2} + \sigma_2^{\,2} + \sigma_3^{\,2} &= \frac{1}{3}\left(2\sigma_1^{\,2} + 2\sigma_2^{\,2} + 2\sigma_3^{\,2} - 2\sigma_1\sigma_2 - 2\sigma_2\sigma_3 - 2\sigma_3\sigma_1\right) \\ &\quad + \frac{1}{3}\left(\sigma_1^{\,2} + \sigma_2^{\,2} + \sigma_3^{\,2} + 2\sigma_1\sigma_2 + 2\sigma_2\sigma_3 + 2\sigma_3\sigma_1\right) \\ &= \frac{1}{3}\left((\sigma_1 - \sigma_2)^2 + (\sigma_2 - \sigma_3)^2 + (\sigma_3 - \sigma_1)^2\right) + \frac{1}{3}\left(\sigma_1 + \sigma_2 + \sigma_3\right)^2\end{aligned} \tag{8}$$

Since $J_{2D} = \frac{1}{6}\left((\sigma_1 - \sigma_2)^2 + (\sigma_2 - \sigma_3)^2 + (\sigma_3 - \sigma_1)^2\right)$, Eq.7 is to be

$$\sigma_1^{\,2} + \sigma_2^{\,2} + \sigma_3^{\,2} = 2J_{2D} + \frac{1}{3} I_1^{\,2} \tag{9}$$

Therefore, Eq. 7 is to be

$$J_{2D} + \frac{3}{2}(\sigma_{11}^{\,2} + \sigma_{22}^{\,2} + \sigma_{33}^{\,2}) + I_2 - \frac{5}{6} I_1^{\,2} = 4J_{2D} + I_2 - \frac{1}{3} I_1^{\,2} \tag{10}$$

Therefore, the final form of the failure surface is to be

$$\frac{2}{3b^2}\left(4J_{2D} + I_2 - \frac{1}{3} I_1^{\,2}\right) = 1 - \frac{I_1^{\,2}}{9a^2} - \frac{2\alpha I_1}{3a^2} - \frac{\alpha^2}{a^2}$$

$$\frac{8}{3b^2} J_{2D} + \frac{2}{3b^2} I_2 - \frac{2}{9b^2} I_1^{\,2} + \frac{I_1^{\,2}}{9a^2} + \frac{2\alpha I_1}{3a^2} + \frac{\alpha^2}{a^2} = 1$$

$$\frac{8}{3b^2} J_{2D} + \frac{2}{3b^2} I_2 + \frac{1}{9}\left(\frac{1}{a^2} - \frac{2}{b^2}\right) I_1^{\,2} + \frac{2\alpha}{3a^2} I_1 + \frac{\alpha^2}{a^2} = 1 \tag{11}$$

or if the calculation will be made in the normal stress plane rather than principal axis, the formulation is the same as Eq. 6 which is:

$$\frac{2}{3b^2}\left(J_{2D} + \frac{3}{2}(\sigma_{11}{}^2 + \sigma_{22}{}^2 + \sigma_{33}{}^2) + I_2 - \frac{5}{6} I_1{}^2 \right) = 1 - \frac{I_1{}^2}{9a^2} - \frac{2\alpha I_1}{3a^2} - \frac{\alpha^2}{a^2} \qquad (6)$$

Therefore

$$\frac{2}{3b^2} J_{2D} + \frac{1}{b^2}(\sigma_{11}{}^2 + \sigma_{22}{}^2 + \sigma_{33}{}^2) + \frac{2}{3b^2} I_2 + \frac{1}{9}\left(\frac{1}{a^2} - \frac{5}{b^2} \right) I_1{}^2 + \frac{2\alpha}{3a^2} I_1 + \frac{\alpha^2}{a^2} = 1 \qquad (12)$$